



USDOT Region V Regional University Transportation Center Final Report

NEXTRANS Project No. 092OY04

## **Increasing Accuracy of Vehicle Detection from Conventional Vehicle Detectors- Counts, Speeds, Classification, and Travel Time**

By

Benjamin Coifman, PhD

Associate Professor  
The Ohio State University  
Department of Civil, Environmental, and Geodetic Engineering  
Department of Electrical and Computer Engineering

Hitchcock Hall 470  
2070 Neil Ave, Columbus, OH 43210

E-mail: [Coifman.1@OSU.edu](mailto:Coifman.1@OSU.edu)

and

Lan Wu  
The Ohio State University  
Department of Civil, Environmental, and Geodetic Engineering

and

Heng Wei, PhD  
Associate Professor,  
The University of Cincinnati  
School of Advanced Structures

## **DISCLAIMER**

Funding for this research was provided by the NEXTRANS Center, Purdue University under Grant No. DTRT07-G-005 of the U.S. Department of Transportation, Research and Innovative Technology Administration (RITA), University Transportation Centers Program. The contents of this report reflect the views of the authors, who are responsible for the facts and the accuracy of the information presented herein. This document is disseminated under the sponsorship of the Department of Transportation, University Transportation Centers Program, in the interest of information exchange. The U.S. Government assumes no liability for the contents or use thereof.



## USDOT Region V Regional University Transportation Center Final Report

# TECHNICAL SUMMARY

NEXTRANS Project No. 092OY04

Final Report, September 23, 2014

## **Increasing Accuracy of Vehicle Detection from Conventional Vehicle Detectors- Counts, Speeds, Classification, and Travel Time**

### **Introduction**

Vehicle classification is an important traffic parameter for transportation planning and infrastructure management. Length-based vehicle classification from dual loop detectors is among the lowest cost technologies commonly used for collecting these data. Like many vehicle classification technologies, the dual loop approach works well in free flow traffic. Effective vehicle lengths are measured from the quotient of the detector dwell time and vehicle traversal time between the paired loops. This approach implicitly assumes that vehicle acceleration is negligible, but unfortunately at low speeds this assumption is invalid and length-based classification performance degrades in congestion.

To address this problem, we seek a solution that relies strictly on the measured effective vehicle length and measured speed. We analytically evaluate the feasible range of true effective vehicle lengths that could underlie a given combination of measured effective vehicle length, measured speed, and unobserved acceleration at a dual loop detector. From this analysis we find that there are small uncertainty zones where the measured length class can differ from the true length class, depending on the unobserved acceleration. In other words, a given combination of measured speed and measured effective vehicle length falling in the uncertainty zones could arise from vehicles with different true length classes. Outside of the uncertainty zones, any error in the measured effective vehicle length due to acceleration will not lead to an error in the measured length class. Thus, by mapping these uncertainty zones, most vehicles can be accurately sorted to a single length class, while the few vehicles that fall within the uncertainty zones are assigned to two or more classes. We find that these uncertainty zones remain small down to about 10 mph and then grow exponentially as speeds drop further.

Using empirical data from stop-and-go traffic at a well-tuned loop detector station the best conventional approach does surprisingly well; however, our new approach does even better, reducing the classification error rate due to acceleration by at least a factor of four relative to the best conventional method. Meanwhile, our approach still assigns over 98% of the vehicles to a single class.

## Findings

Dual loop detectors are among the lowest cost technologies commonly used for collecting vehicle classification data. The conventional approach to classify vehicles at dual loop detectors implicitly assumes that vehicle acceleration is negligible; but unfortunately, at low speeds this assumption is invalid. As a result of this fact, many operating agencies are reluctant to deploy classification stations on roadways where traffic is frequently congested.

This work sought to address the impacts of the unobserved acceleration on the measured length class. After calibration, the approach relies strictly on the measured effective vehicle length and measured speed at a conventional dual loop detector. To this end, the work established the uncertainty regions where the true vehicle class is ambiguous based on what can actually be measured from a dual loop detector. Using the equations of motion this work analytically derived the set of true vehicle lengths, speeds, and accelerations that could give rise to a particular combination of measured speed and measured effective vehicle length. Of course acceleration cannot be measured from conventional dual loop detectors and this analysis found that there are small uncertainty zones where the measured length class can differ from the true length class, depending on the unobserved acceleration. In other words, a given combination of measured speed and measured effective vehicle length falling in the uncertainty zones could arise from vehicles with different true length classes. In other words, the uncertainty zones capture the impacts of the unmeasured acceleration. Outside of the uncertainty zones, any error in the measured effective vehicle length due to acceleration will not lead to an error in the measured length class. Thus, by mapping these uncertainty zones, most vehicles can be accurately sorted to a single length class, while the few vehicles that fall within the uncertainty zones are assigned to two or more classes. Using empirical data from stop-and-go traffic we found that this new approach assigns over 98% of the vehicles to a single class, and reduces the classification error rate by at least a factor of four relative to the best conventional constant speed boundary method.

Contrary to conventional wisdom we found that the conventional, constant speed boundaries performed surprisingly well down to 15 mph for both of the empirical evaluation datasets.

The uncertainty zone method presented in this work is meant to extend meaningful length-based vehicle classification to sites that see some congestion. Reviewing the data, the stop case and even some of the low speed, non-constant acceleration cases can yield very large errors in the measured effective vehicle lengths. Fortunately, these errors are somewhat rare for several reasons, first, very few vehicles actually pass the dual loop detector at these low speeds, since the lower the speed the lower the flow and the lower the flow the fewer vehicles actually pass a detector. Second, as shown in the report, the uncertainty zones only impact measured effective vehicle lengths above 26 ft. There is no uncertainty for any vehicles with a measured effective vehicle length below the zones, no matter how low the measured speed is. Meanwhile, for a measured speed below 8 mph, the work found that almost all measured effective vehicle lengths above 26 ft will fall in the uncertainty zones.

## Recommendations

The present work seeks to demonstrate just how small the uncertainty zones are. It is left to future work to derive a universal expression to specify the uncertainty zone boundaries for different length bins or dual loop detector spacing. Although we found slightly higher error rates when using the real loop detector data than the purely synthetic data, the difference was very small, i.e., the performance from the NGSIM synthetic transition times was similar to those from the well tuned loop detectors in the Berkeley Highway Laboratory. So for some other set of length bins and dual loop spacing, one could simply repeat the analytical processed developed in this report and evaluate the results strictly using the NGSIM data. While our work only used the NGSIM I-80 dataset due to the overlap with the BHL, there is a second NGSIM freeway dataset from US-101 that could also be used. In either case, the NGSIM data come from urban freeways with the majority of vehicles being passenger cars. Fortunately, the classification of one vehicle is independent of the classification of another vehicle at a well tuned detector. So if one were interested strictly in the longer vehicles, one could simply discount the class 1 vehicles. To increase the proportion of observations arising from long vehicles, the simulated loop detectors could be deployed at multiple locations along one of the NGSIM corridors to generate the synthetic transition data in an effort to sample the limited number of trucks under different acceleration conditions.

## Contacts

*For more information:*

Benjamin Coifman, PhD  
The Ohio State University  
Department of Civil, Environmental, and Geodetic Engineering  
Hitchcock Hall 470  
2070 Neil Ave, Columbus, OH 43210

(614) 292-4282  
Coifman.1@OSU.edu

<https://ceg.osu.edu/~coifman>

**NEXTRANS Center**  
Purdue University - Discovery Park  
3000 Kent Ave  
West Lafayette, IN 47906

[nextrans@purdue.edu](mailto:nextrans@purdue.edu)  
(765) 496-9729  
(765) 807-3123 Fax

[www.purdue.edu/dp/nextrans](http://www.purdue.edu/dp/nextrans)

## TABLE OF CONTENTS

	Page
LIST OF FIGURES .....	ii
LIST OF TABLES .....	iii
CHAPTER 1. INTRODUCTION .....	1
1.1 Effective Vehicle Length Measurement and Length Classes .....	3
CHAPTER 2. VEHICLE CLASSIFICATION IN THE PRESENCE OF ACCELERATION .....	6
2.1 Establishing the Range of Acceleration .....	7
2.2 Measured Class Boundaries Given a Constant Speed .....	7
2.3 Measured Class Boundaries Given a Non-Stop Constant Acceleration .....	8
2.4 Measured Class Boundaries Given a Non-constant Acceleration .....	8
2.5 Measured Class Boundaries Given a Stop Over the Dual Loop Detector .....	9
2.6 Class Boundaries without Knowledge of the Acceleration .....	11
CHAPTER 3. PERFORMANCE EVALUATION USING EMPIRICAL DATA .....	17
3.1 Evaluation from NGSIM .....	18
3.2 Evaluation from BHL .....	19
CHAPTER 4. DISCUSSION AND CONCLUSIONS .....	31
REFERENCES .....	35

## LIST OF FIGURES

Figure	Page
Figure 1.1. Schematic of a vehicle passing over a dual detector showing the four transition times that comprise the response of the two detectors and the resulting measurements used to calculate speed and length. ....	5
Figure 2.1. Acceleration distribution from all vehicles in the NGSIM I-80 dataset. ....	12
Figure 2.2. Vehicle classification boundaries for, (a) the constant speed model, (b) the constant acceleration model, (c) the non-constant acceleration model, and (d) the stop model. ....	13
Figure 2.3. Time series speed of an individual vehicle for (a) the non-constant acceleration model, (b) the stop model. ....	14
Figure 2.4. Theoretical uncertainty zones in the measured length and speed plane when acceleration is equal to (a) $\pm 1$ mphps, (b) $\pm 2$ mphps, and (c) $\pm 4$ mphps. ....	15
Figure 2.5. The length-based vehicle classification plane showing the uncertainty zones where errors in the measured length could lead to a misclassification if one only used the conventional constant speed boundaries. The numbers on this plot denote the vehicle classes that fall within the given area. ....	16
Figure 3.1. (a) Scatter plot comparing the measured length and classification from the synthetic NGSIM detector data versus the true NGSIM length and class at the study location, (b) CDF of average measured speeds for the same vehicles. ....	27
Figure 3.2. (a) Vehicle classification using measured effective vehicle length versus measured speed for all of the NGSIM data at 1,000 ft, (b) repeating part a, but only showing the one misclassification that falls outside of the correct region or uncertainty zones. ....	28
Figure 3.3. (a) Scatter plot comparing the measured length and classification from the real BHL loop detector Station 8 data versus the corresponding true NGSIM length and class, (b) CDF of average measured speeds for the same vehicles. ....	29
Figure 3.4. (a) Vehicle classification using measured effective vehicle length versus measured speed for all of BHL loop detector Station 8 data, (b) repeating part a, but only showing the one misclassification that falls outside of the correct region or uncertainty zones. ....	30

## LIST OF TABLES

Table	Page
Table 3.1. Using the synthetic detectors from NGSIM at 1,000 ft, the left-hand side of this table compares the measured length class when including the uncertainty zones against the true length class. The right-hand side of this table repeats a comparison using only the conventional constant speed boundaries between classes. ....	23
Table 3.2. Repeating the analysis for CM using the synthetic detectors from NGSIM at 1,000 ft, comparing the conventional constant speed boundaries between classes against the true length class. ....	24
Table 3.3. Using the real detector data from BHL loop detector Station 8, the left-hand side of this table compares the measured length class when including the uncertainty zones against the true length class. The right-hand side of this table repeats a comparison using only the conventional constant speed boundaries between classes. ....	25
Table 3.4. Repeating the analysis for CM using the real detector data from BHL loop detector Station 8 comparing the conventional constant speed boundaries between classes against the true length class. ....	26

## CHAPTER 1. INTRODUCTION

Vehicle classification is an important traffic parameter for transportation planning and infrastructure management. Length-based vehicle classification from dual loop detectors is among the lowest cost technologies commonly used for collecting these data. A dual loop detector station typically consists of a pair of loop detectors separated by a known distance in each lane. In conventional practice, speed is the quotient of this known distance between the loop detectors and a given vehicle's measured traversal time between the paired detectors. The product of this speed measurement and the dwell time over one of the detectors is then used to calculate the effective vehicle length (where the effective vehicle length is the sum of the physical vehicle length and the size of the loop's detection zone). Finally, to classify the vehicle, each of these effective vehicle length measurements is then sorted into one of several different length bins, e.g., a three bin scheme might seek to sort passenger vehicles, single unit trucks, and multiple unit trucks into different bins.

Like many vehicle classification technologies, the dual loop approach works well in free flow traffic (Davies and Salter, 1983; Minge et al., 2012; Kim and Coifman, 2013). This approach implicitly assumes that vehicle acceleration is negligible; but unfortunately, at low speeds this assumption is invalid (e.g., Wu and Coifman, in press) and performance degrades significantly in congestion (Davies and Salter, 1983; Wu and Coifman, in press). As a result of this fact, many operating agencies are reluctant to deploy classification stations on roadways where traffic is frequently congested.

To address this problem, we seek a solution that relies strictly on the measured effective vehicle length and measured speed. We first use the equations of motion to

synthesize hypothetical loop detector data and evaluate the feasible range of true effective vehicle lengths that could underlie a given combination of measured effective vehicle length and measured speed at a dual loop detector as the unobserved acceleration is varied. From this analysis we find that there are small uncertainty zones where the measured length class can differ from the true length class, depending on the unobserved acceleration. In other words, a given combination of measured speed and measured effective vehicle length falling in the uncertainty zones could arise from vehicles with different true length classes. Outside of the uncertainty zones, any error in the measured effective vehicle length due to acceleration will not lead to an error in the measured length class. Thus, by mapping these uncertainty zones, most vehicles can be accurately sorted to a single length class, while the few vehicles that fall within the uncertainty zones are assigned to two or more classes. We find that these uncertainty zones remain small down to about 10 mph and then grow exponentially as speeds drop further. Then using empirical data from stop-and-go traffic we evaluate the performance of this new approach, first via synthetic detector data, and then using data from a real dual loop detector station.

The remainder of this section briefly reviews the conventional dual loop detector effective vehicle length measurement and vehicle classification used in this work. As noted above, this conventional method for measuring effective vehicle length assumes that acceleration is negligible. Section 2 uses the equations of motion to evaluate the impacts of unaccounted for acceleration and complete stops on the conventional effective vehicle length measurement. The section generates synthetic vehicle trajectories and then finds the pairwise combinations of measured effective vehicle length and measured speed from a simulated dual loop detector to identify the uncertainty zones where the unaccounted for acceleration can cause the measured effective vehicle length to result in a different classification than the true effective vehicle length would fall in. Once the uncertainty zones have been established, deviating from conventional practice, measurements that fall in these zones are assigned either two or three possible vehicle classes that correspond to the given uncertainty zone. Section 3 evaluates the

performance of the new methodology using empirical data. Finally, this report closes with a discussion and conclusions in Section 4.

### 1.1 *Effective Vehicle Length Measurement and Length Classes*

Figure 1.1 shows the time-space representation of a vehicle passing over a dual loop detector, with the paired loops separated by spacing  $S$  (leading edge to leading edge). The loop detector controller records four transition times, denoted  $t_1$  to  $t_4$ , as the vehicle enters and leaves the two detection zones. From which the controller then calculates the traversal times from the rising edges,  $TT_r = t_3 - t_1$ , and falling edges,  $TT_f = t_4 - t_2$ , which in turn yield two separate measures of speed:  $V_r = S/TT_r$  and  $V_f = S/TT_f$ . Similarly, there are two measures dwell time: over the first detector,  $T_u = t_2 - t_1$ , and second detector,  $T_d = t_4 - t_3$ , as shown in the figure. As discussed in Wu and Coifman (in press), in conventional practice there are several different ways of averaging these speeds and dwell times to calculate the effective vehicle length. This earlier work evaluated the various combinations in the presence of accelerations and found the method from Coifman and Cassidy (2002) (denoted CM+ and given by Equation 1) proved to be the most robust variant of the conventional method during stop-and-go traffic conditions. Note that the "+" suffix denotes the fact that CM+ is already better than the most commonly used conventional approach, CM, that uses just one pair of the speed and dwell time measurements, as given by Equation 2. Wu and Coifman found that the length-based classification error rate from CM+ was roughly half that of CM.

$$L_{CM+} = \frac{V_r * T_u + V_f * T_d}{2} \quad (1)$$

$$L_{CM} = V_r * T_u \text{ or } L_{CM} = V_f * T_d \quad (2)$$

In this work, for illustration purposes we adopt the classification length bins commonly used by the Ohio Department of Transportation (ODOT), as discussed in Coifman and Kim (2009), and repeated below. Meanwhile, Section 4 will discuss how to extend this work to other length bins.

Class 1:  $0 \text{ feet} < \text{effective vehicle length} \leq 28 \text{ feet}$

Class 2:  $28 \text{ feet} < \text{effective vehicle length} \leq 46 \text{ feet}$

Class 3:  $\text{effective vehicle length} > 46 \text{ feet}$

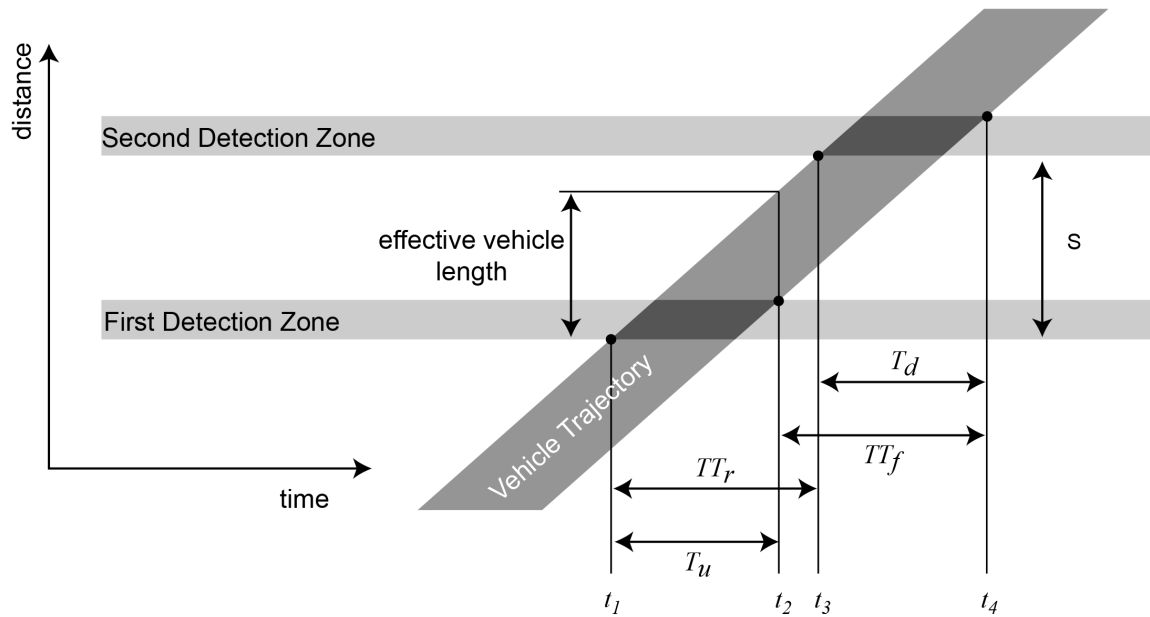


Figure 1.1. Schematic of a vehicle passing over a dual detector showing the four transition times that comprise the response of the two detectors and the resulting measurements used to calculate speed and length.

## CHAPTER 2. VEHICLE CLASSIFICATION IN THE PRESENCE OF ACCELERATION

As noted above, the conventional method for measuring effective vehicle length assumes that acceleration is negligible. In the following subsections we investigate the impacts of the unaccounted for acceleration using the equations of motion to synthesize hypothetical loop detector data and evaluate the feasible range of true effective vehicle lengths that could underlie a given combination of measured effective vehicle length, measured speed, and unobserved acceleration at a dual loop detector. We evaluate four specific vehicular movements: constant speed, constant acceleration, non-constant acceleration, and coming to a complete stop. In each case we investigate the impacts the given vehicle movement will have on the effective vehicle length measurement from Equation 1, with specific attention to the situations where the resulting measured length class can differ from the true length class. Each of these four movement models is first considered individually, and then we combine the results to establish the boundaries of the classification uncertainty zones. For each of the movement models we choose a vehicle's true effective vehicle length, initial speed, and acceleration profile; synthesized the resulting transition times shown in Figure 1.1; calculated the average measured speed from Equation 3 and effective vehicle length from Equation 1; and then compared the measured length class to the true length class. We present the results in the measured effective vehicle length versus measured speed plane to put them in the context of metrics that can be measured directly at conventional dual loop detectors. In most cases it is sufficient to evaluate the boundary values between vehicle classes, i.e., 28 ft and 46 ft used in this report.

$$\bar{V} = \frac{V_r + V_f}{2} \quad (3)$$

### 2.1 Establishing the Range of Acceleration

To establish the range of reasonable acceleration for this work, we employ one of the Next Generation Simulation (NGSIM) datasets. The NGSIM program was initiated by the Federal Highway Administration (FHWA) to collect high-quality, empirical vehicle trajectory data to support the development of better traffic simulation (Kovvali et al., 2007). In particular, we use the I-80 dataset, which includes vehicle trajectories on a 1,650 ft long segment of I-80 in Emeryville, California for 45 min during the evening peak on April 13, 2005. Figure 2.1 shows the probability mass function of the accelerations recorded for all vehicles, at all locations in the NGSIM dataset. Over 70% of the accelerations range from -2mphps to 2 mphps, and over 50% range from -1 to +1 mphps. In fact there is considerable evidence in the literature to suggest that the magnitudes of the NGSIM accelerations are too large, e.g., Punzo et al (2011). Montanino and Punzo (2013) found that after correcting the NGSIM I-80 dataset, roughly 90% of the accelerations fell within  $\pm 2$  mphps. So in the following sections we use  $a = \pm 1$  mphps or  $a = \pm 2$  mphps as our reference values.

### 2.2 Measured Class Boundaries Given a Constant Speed

The simplest vehicle motion is the constant speed model, whereby the vehicle passes a dual loop detector with a constant speed. In this case, there is no acceleration and the vehicle does not stop while traversing the detector, thus  $V_r = V_f$  and  $T_u = T_d$ . So the measured effective vehicle length from Equation 1 should equal the true effective vehicle length for the given vehicle. Therefore, under constant speed the boundaries between measured length classes are equal to the boundaries between the true length classes for all measured speeds. The bold lines in Figure 2.2a show these boundaries between the measured length classes.

### 2.3 Measured Class Boundaries Given a Non-Stop Constant Acceleration

The simplest vehicle motion that includes acceleration is one of constant acceleration, with no stops over the dual detector. For the boundary between class 1 and 2 we set the true effective vehicle length,  $L_e$ , to be 28 ft, and for the boundary between class 2 and 3 we set  $L_e$  to be 46 ft. Setting the loop spacing,  $S$ , to be 20 ft, we vary the true initial speed,  $V_0$ , from 0 to 100 mph, at  $\Delta V = 0.1$  mph increments, and set acceleration,  $a$ , to +2 mphps and -2 mphps. Synthesizing the detector transition times from Figure 1.1, then calculating the measured speed from Equation 3 and measured effective vehicle length from Equation 1, the bold curves in Figure 2.2b show how the boundary curves between the true length classes are pulled to shorter effective vehicle lengths as speeds approach the stop region in the presence of a constant acceleration. These curves are truncated when they hit the shaded region, denoting the threshold where the given vehicle would come to (or start from) a stop at the given acceleration. Note that the average measured speed differs from  $V_0$ , and in this case positive and negative accelerations both lead to very similar boundary curves. Within the non-stop region the resulting error in the boundary curve from the measured effective vehicle length is small down to 10 mph and then starts to grow as the average speed drops, until reaching the edge of the stop region. The general shape of the boundaries between classes and the threshold of the stop region remain the same at different values of  $|a|$ , but as  $|a|$  shrinks, the associated speeds also drop, and the curves compress to the left.

### 2.4 Measured Class Boundaries Given a Non-constant Acceleration

To capture the non-constant acceleration case we use a piecewise linear acceleration profile as shown in Figure 2.3a for a given vehicle passing over the dual loop detector. This model is characterized by the accelerations,  $a_i$  and  $a_j$ ; initial speed,  $V_0$ ; and the speed at the inflection point,  $V_x$ ; while the two time periods,  $t_i$  and  $t_j$  denote the time spent by the vehicle during the given acceleration and can be expressed as a function of the other variables. For illustrative purposes we consider the four following combinations:

- scenario 1,  $a_i = 1$  mphps, and  $a_j = 2$  mphps;
- scenario 2,  $a_i = 2$  mphps, and  $a_j = -2$  mphps;
- scenario 3,  $a_i = -2$  mphps, and  $a_j = 2$  mphps; and
- scenario 4,  $a_i = -1$  mphps, and  $a_j = -2$  mphps.

In this model we set  $t_i = t_j$  and vary  $V_x$  from 0 to 100 mph, at  $\Delta V = 0.1$  mph increments (excluding all combinations that would yield a negative  $V_0$  or final speed at time  $t_f$  in Figure 2.3a). Hence, for each case the initial speed  $V_0$  is calculated from  $a_i$ ,  $a_j$ ,  $L_e$ ,  $S$  and  $V_x$ , and once more we synthesize the detector transition times. Figure 2.2c shows the range of outcomes from the two boundary curves, mapping out an uncertainty zone between the distinctly discernable length classes. For both uncertainty zones the top right of the zone comes primarily from scenario 2, the lower edge of the zone arises primarily from scenarios 1 and 4, and the left edge of the uncertainty zone from scenario 3, corresponding to the edge of the stop region when  $V_x=0$ .<sup>1</sup> So in this case, at 20 mph the lower uncertainty zone exhibits a range of 1.2 ft and the upper uncertainty zone exhibits a range of 1.9 ft. At 15 mph these zones grow to 2.0 ft and 3.8 ft, respectively. The top of the uncertainty zones quickly exceeds the maximum feasible vehicle length as speeds drop further, and in the case of the lower zone actually bends back towards higher measured speeds at longer measured effective vehicle lengths.

### 2.5 Measured Class Boundaries Given a Stop Over the Dual Loop Detector

So far we have considered acceleration in the absence of stops, but in stop-and-go traffic, vehicles will stop over the dual loop detector. Because  $L_e > S$  for both boundaries, when one of these vehicles stop it will do so over one or both of the loop detectors. First, consider the case where the vehicle stops over the upstream detector, before reaching the downstream detector. In the context of Figure 1.1,  $t_1$  will move to the left by the duration of the stop time, impacting both  $TT_r$  and  $T_u$ . In this case the effective vehicle length measurement error will be relatively small because these extensions from the stop time

---

<sup>1</sup> Because this plot uses four different combinations of accelerations, the stop region boundary is no longer a well-defined curve, as it was in Figure 2.2b

partially cancel each other out via CM+ in Equation 1. On the other hand if the vehicle stops over both detectors, both  $t_1$  and  $t_3$  will move to the left by the duration of the stop time.<sup>2</sup> So now both dwell times will be extended by the stop time, but neither traversal time will include the stop time. This imbalance will lead to a large error by CM+ in Equation 1 and the measured effective vehicle length will be much longer than the true effective vehicle length. Similarly, if one only used CM from Equation 2, the errors can also persist when a vehicle stops over just one detector.

Extending the non-constant acceleration model to include a stop time, we use the piecewise linear acceleration profile shown in Figure 2.3b for a vehicle stopping over the dual loop detector at the worst possible location relative to the loops, i.e., with the vehicle stopped over both loops and centered relative to the two loops. The only things that we change from Section 2.4 is the addition of the stop time,  $\Delta t$ , we only consider the stop region ( $V_x=0$ ), and now we only use scenario 3 because it traces out the lower bound of the uncertainty zones. The bold curves in Figure 2.2d show the case when  $\Delta t = 0$ , which means the vehicle comes to a complete stop over the detection zone and then immediately accelerates away. For speeds just below the right hand edge of the stop region we see the boundary drops to the lowest measured effective vehicle length and then quickly shoots up beyond the largest feasible vehicle (while also moving to higher average measured vehicle speed). Keep in mind that this is the lower bound of the class above for the given acceleration profile, with the upper bound already being established in Figure 2.2c. For longer  $\Delta t$  the two boundaries in Figure 2.2d shift to lower measured speeds and effective vehicle lengths.

After including non-zero stop times and vehicles that come to a stop over just one loop, most measurements falling in the stop region with measured effective vehicle length between 26 ft and 42 ft could come either from a class 1 or class 2 vehicle, while a measured effective vehicle length above 42 ft could come from a vehicle in any one of the three classes.

---

<sup>2</sup> Note that Figure 1.1 illustrates the case with  $L_e < S$ ,  $t_2$  and  $t_3$  will swap their temporal order whenever  $L_e > S$ .

## 2.6 Class Boundaries without Knowledge of the Acceleration

Figure 2.4b shows the intersection of all of the boundaries from Figure 2.2, with  $|a| = 2 \text{ mphps}$ . Figure 2.4a repeats this analysis except now  $|a| = 1 \text{ mphps}$  and Figure 2.4c repeats in analysis with  $|a| = 4 \text{ mphps}$ . The three plots exhibit a similar shape; however, as the magnitude of acceleration increases, the curves shift to the right and the inclination increases, reflecting the impacts of acceleration on the effective vehicle length measurement accuracy. Figures 2.2 and 2.4b arise from the same specific choice of the acceleration profile. In general the acceleration profile cannot be measured from a dual loop detector and each vehicle likely chooses its own profile without regard to the average conditions used thus far in our analysis. Capturing the resulting measured effective vehicle lengths and speeds from all feasible accelerations, Figure 2.5 steps through acceleration magnitudes from 0 to 4 mphps and records all of the possible true vehicle classes observed at the given point on measured effective vehicle length and speed plane.<sup>3</sup> The three shaded regions: ABHG, BCDH and GHEF, bound the measured speed and measured effective vehicle length pairs that could arise from vehicles of multiple true classes, namely: classes 1&2&3, 2&3, and 1&2, respectively. The remainder of the plane is un-shaded, denoting that in the absence of detector errors those measured speed and measured effective vehicle length pairs could only arise from a single true vehicle class.

---

<sup>3</sup> This figure includes constant acceleration with  $|a| \leq 4 \text{ mphps}$ , as well as non-constant acceleration and stopped vehicles with  $|a_i| + |a_j| \leq 4 \text{ mphps}$ .

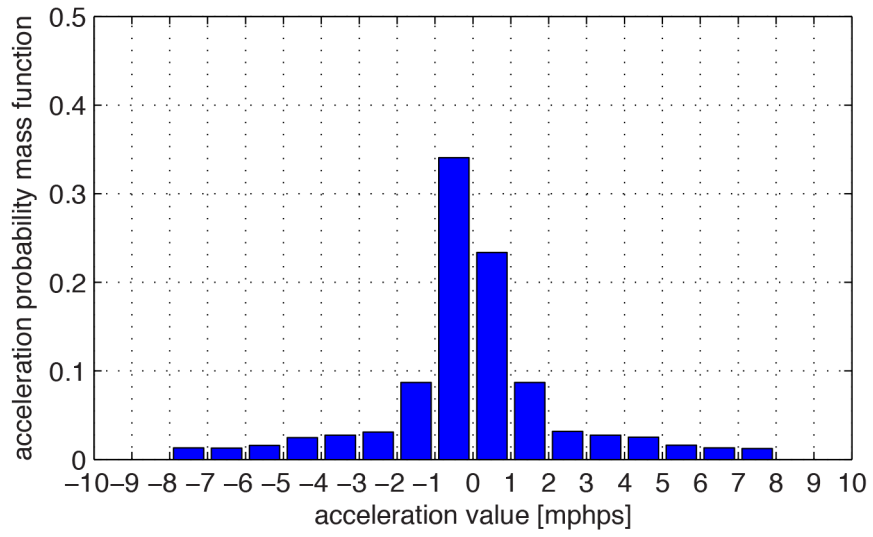


Figure 2.1. Acceleration distribution from all vehicles in the NGSIM I-80 dataset.

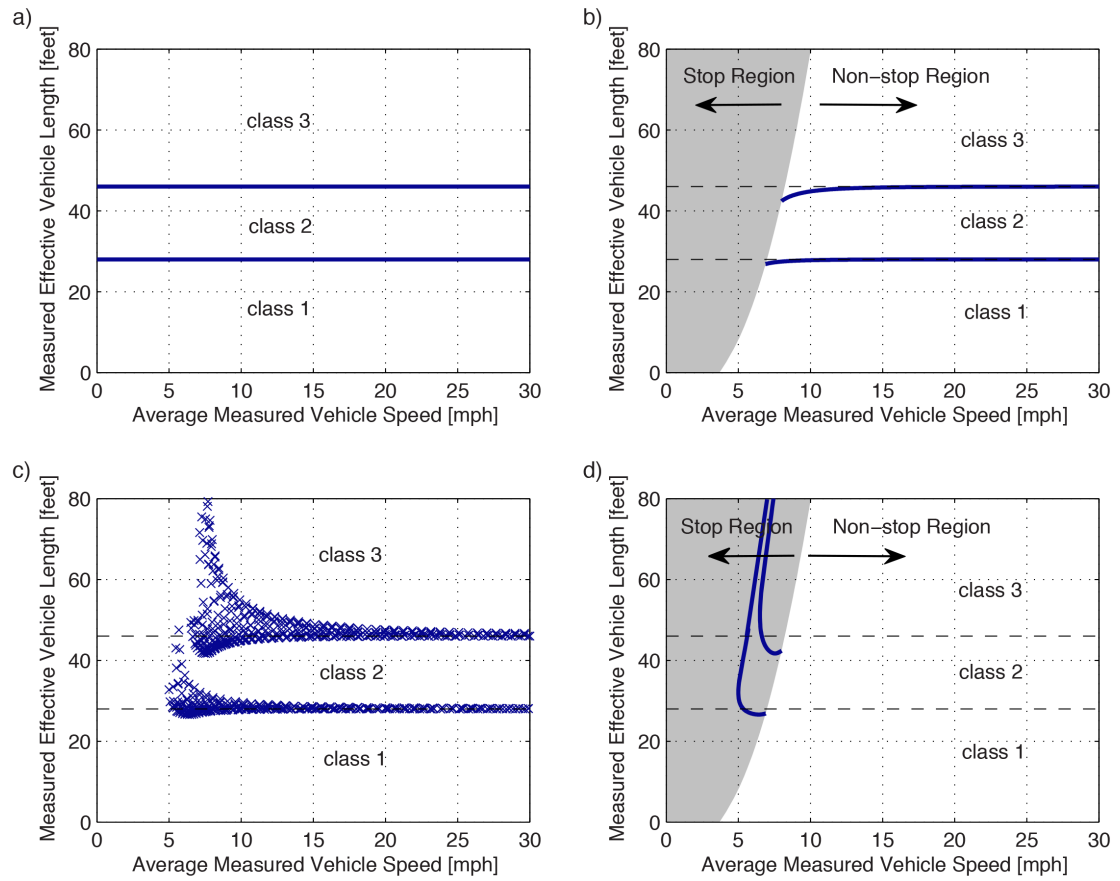


Figure 2.2. Vehicle classification boundaries for, (a) the constant speed model, (b) the constant acceleration model, (c) the non-constant acceleration model, and (d) the stop model.

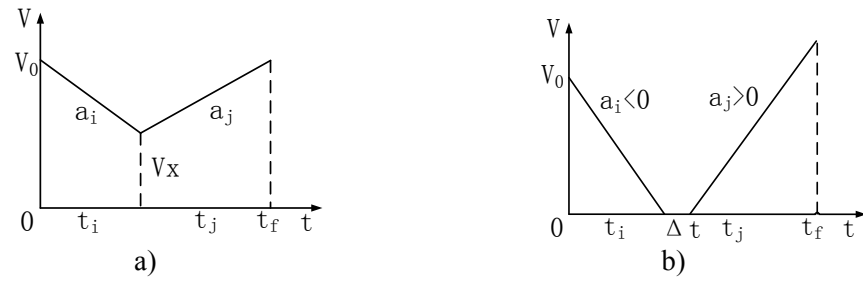


Figure 2.3. Time series speed of an individual vehicle for (a) the non-constant acceleration model, (b) the stop model.

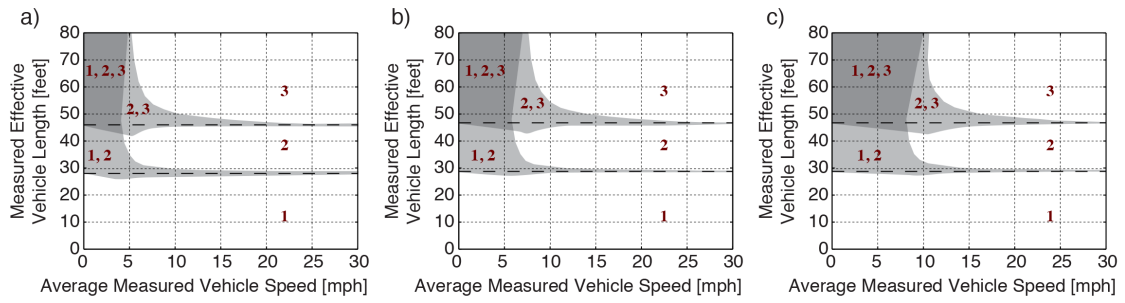


Figure 2.4. Theoretical uncertainty zones in the measured length and speed plane when acceleration is equal to (a)  $\pm 1$  mphps, (b)  $\pm 2$  mphps, and (c)  $\pm 4$  mphps.

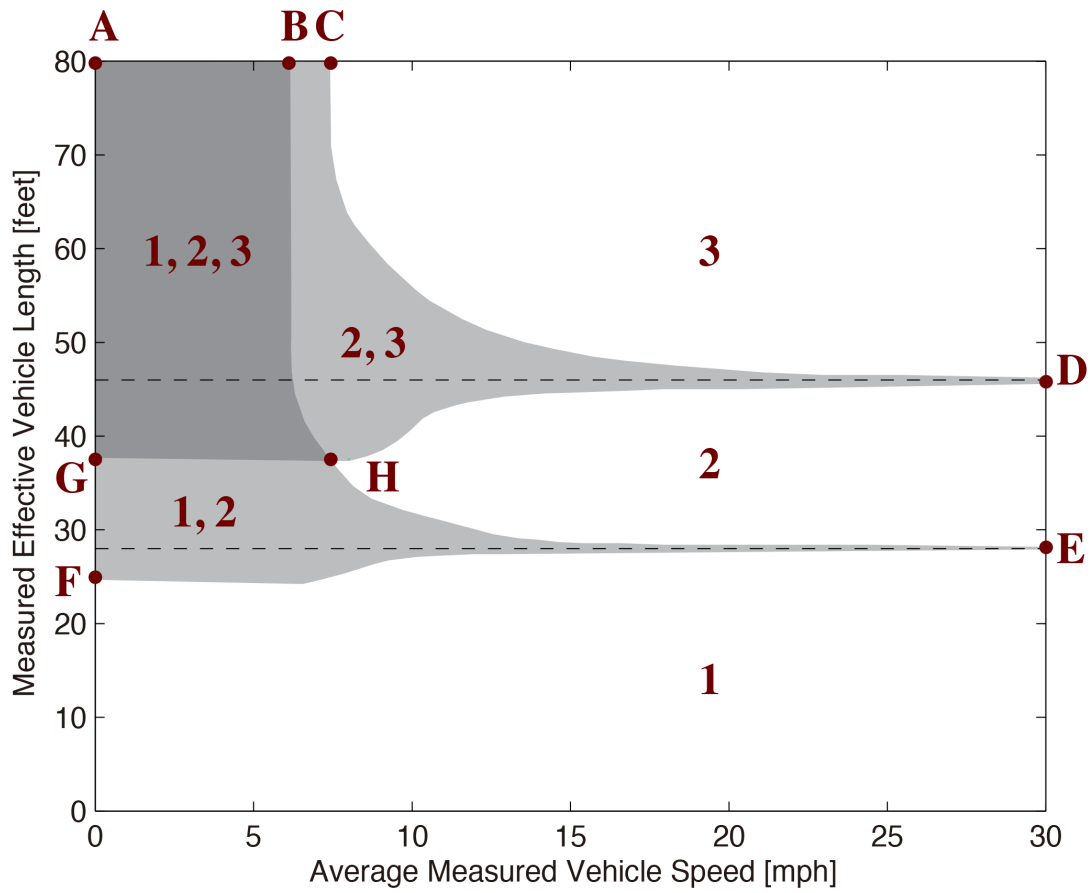


Figure 2.5. The length-based vehicle classification plane showing the uncertainty zones where errors in the measured length could lead to a misclassification if one only used the conventional constant speed boundaries. The numbers on this plot denote the vehicle classes that fall within the given area.

### CHAPTER 3. PERFORMANCE EVALUATION USING EMPIRICAL DATA

There are very few publicly available, empirical datasets that include the necessary transition times ( $t_1$  to  $t_4$  in Figure 1.1) from dual loop detector data. There are even fewer datasets that include ground truth vehicle lengths for vehicles in stop-and-go traffic. To evaluate the length-based classification scheme we use two empirical data sources. The first empirical dataset is the NGSIM I-80 data mentioned above, from which we simulate a dual loop detector station and extract synthetic transition times from all of the passing vehicles. Since the NGSIM data includes the vehicle trajectories and vehicle lengths, the synthetic transition times capture the impacts of vehicle length, speed, and acceleration. From which, we can then measure the errors arising from the dual loop measurements (Equations 1 and 3).

The second empirical dataset comes from an actual dual loop detector station, namely Station 8 in the Berkeley Highway Laboratory, BHL (Coifman et al., 2000). Unlike conventional practice, the BHL dual loop detector stations recorded the individual vehicle transition times, allowing for direct application of Equations 1 and 3 to the archived data. Meanwhile, BHL Station 8 has a small amount of data with concurrent ground truth vehicle lengths because it falls within the surveillance region of the NGSIM I-80 dataset. Although this station was off-line for most of the time that the NGSIM data were collected, there are about 12 minutes of BHL dual loop detector data with concurrent NGSIM ground truth vehicle lengths, and this period is used to evaluate the performance from the actual loop detector data.

### 3.1 *Evaluation from NGSIM*

This section uses the NGSIM I-80 dataset to evaluate the classification scheme. We simulated a dual loop detector in each lane, with the leading edge of the upstream loop detector located at 1,000 ft in the NGSIM coordinate system. The detection zone size was set to 6 feet for each loop detector, with  $S = 20$  ft. A total of 5,675 vehicles passed this location. Transition times  $t_1$  and  $t_3$  come directly from the NGSIM trajectory data as the vehicle passes the leading edge of each simulated loop detector, while transition times  $t_2$  and  $t_4$  come from a given vehicle's trajectory shifted upstream in space by the vehicle's physical length and the size of the detection zone. The raw NGSIM data are sampled at 10 Hz, and the resulting 1/10 sec uncertainty in the transition times would be much too large to calculate accurate vehicle speeds or effective vehicle lengths from Equations 1-3 at high speeds. So the 10 Hz trajectories are linearly interpolated to find the exact passage time. This approach ignores acceleration because its impact over 1/10 sec should yield a positioning error less than 1/50 ft.<sup>4</sup> The four synthetic transition times are then used to measure effective vehicle length and average measured speed for the given vehicle via Equations 1 and 3. The true effective vehicle length,  $L_e$ , comes from the recorded NGSIM vehicle length plus the size of the detection zone (Wu and Coifman, in press).

Figure 3.1a shows a scatterplot of the measured versus true effective vehicle length. The solid horizontal and vertical lines in the plot show the boundaries between adjacent conventional vehicle classes (as per Section 1.1) relative to the effective vehicle length. Different symbols are used to denote whether the given vehicle was correctly classified into a single class (points) or multiple classes (circles); or was incorrectly classified (cross). Figure 3.1b shows the cumulative distribution function (CDF) of the average measured speed at this detector location. With a median speed of 17 mph and 80% of the speeds below 25 mph, there was considerable congestion, but as can be seen

---

<sup>4</sup> The distance traveled over 1/10 sec is relatively insensitive to acceleration at any speed, allowing us to use linear interpolation to find the synthetic transition times with high accuracy. On the other hand, when measuring speed or length from a dual loop detector, a low speed vehicle will be over the detector for many seconds, and given this long time period acceleration becomes significant.

in Figure 3.1a, most of the vehicles are already correctly classified using CM+ and the conventional constant speed boundaries, without making any accommodation for acceleration.

Figure 3.2a plots the measured effective vehicle length (Equation 1) versus the measured speed (Equation 3) for each of these vehicles, sorted by the true vehicle class as denoted with the given marker symbol. Consistent with Figure 3.1a, most of these vehicles are already correctly classified using the constant speed boundaries shown with dashed horizontal lines. Superimposed on top of this plot are the uncertainty zones from Figure 2.5. Most of the vehicles falling in these uncertainty zones were already correctly classified using the constant speed boundaries; however, most of the vehicles that would have been misclassified using the constant speed boundaries also fall within these uncertainty zones. Figure 3.2b shows the one misclassification that remains after excluding all of the vehicles that were correctly classified either into a single class or to an uncertainty zone that included the correct class. Table 3.1 quantifies these results. The right-hand side shows the results using CM+ and the conventional constant speed boundaries: only seven vehicles are misclassified. These results are probably a little better than one would expect to see at a real detector station since the measurement process excluded the possibility of detector errors from occurring. For reference, Table 3.2 repeats the evaluation using CM from Equation 2 and the conventional constant speed boundaries. The error rate increases to 34 misclassifications (0.6%).

In any event, the left-hand side of Table 3.1 shows the results from CM+ after accounting for the uncertainty zones. A total of 58 vehicles (just over 1%) are assigned to two or more classes. The number of misclassified vehicles dropped to just 1 (improved by a factor of 7 over CM+ with the constant speed boundaries, and a factor of 34 over CM with the constant speed boundaries) when using the uncertainty zones.

### 3.2 *Evaluation from BHL*

The second empirical dataset used in this work comes from an actual dual loop detector station. Namely BHL Station 8, that was within the field of view of the NGSIM

I-80 dataset. There were about 12 minutes of Station 8 dual loop detector data with concurrent ground truth vehicle lengths from NGSIM.

Initially the exact location of Station 8 relative to the NGSIM coordinate system was unknown beyond the fact that the detectors were upstream of the Powell St. on-ramp located at 420 ft in the NGSIM coordinate system. Likewise, the time offset between the two databases was unknown. So we relied upon a brute force, exhaustive search to find the best combination of spatial and temporal offsets. First we synthesized dual loop detector data in every lane from the NGSIM trajectories (as per the method in Section 3.1). This extraction was repeated at many locations along the NGSIM coordinate system, stepping the location of the synthetic dual loop detectors by one foot increments between each successive trial. Using a window of  $\pm 3$  min, each of these synthetic detector stations was compared to the actual dual loop detector data using the method from Lee and Coifman (in press) to find the temporal offset yielding the best correlation between the two data streams, independently in each lane. Then, using these temporal offsets, the location with the best overall correlation, 221 ft, was selected as the location of the actual detector station.

The process of matching the loop data to NGSIM was complicated by the fact that NGSIM sometimes does a poor job tracking the vehicles, e.g., during stop waves it was often the case that one of the NGSIM trajectories would overrun the trajectory of the vehicle ahead of it, erroneously indicating that two vehicles occupied the same point in time and space. Meanwhile, the loop detectors also appear to exhibit splashover problems and all non-vehicle pulses due to splashover were excluded. So after correlating the spatial and temporal offsets between the two concurrent datasets, a second pass was made through to manually match the synthetic pulses to the real detector pulses.

A total of 1,090 vehicles were seen in both datasets. To establish the size of the loop detection zone we took the difference between the measured effective vehicle length from the loops and the corresponding NGSIM reported physical length for the given

vehicle and calculated the average bias, which corresponded to a 7 ft detection zone.<sup>5</sup> We also used the NGSIM synthetic transition data at the exact location of the actual loop detectors (first used to find the spatial and temporal offsets, noted above) and measured the effective vehicle length from the synthetic transition data to capture the impacts of vehicle acceleration. Here too, the bias between the loops and synthetic data corresponded to a 7 ft detection zone. For the remainder of the analysis the *true effective vehicle length* is set to the NGSIM reported physical length plus the 7 ft detection zone.

Upon first comparing the loop data to the concurrent NGSIM measured effective vehicle lengths we found 16 miss-classifications using the measured effective vehicle lengths and constant speed boundaries. Reviewing these errors, we found six cases where the NGSIM effective vehicle length was close to one of the length boundaries and was measured incorrectly on the wrong side of the given boundary. We also found six cases of combined splashover (Lee and Coifman, 2012a) where the splashover event extended the duration of an otherwise valid vehicle actuation; thus, leading to a misclassification. Since the splashover errors and NGSIM length measurement errors are unrelated to the low speed conditions that are the focus of the present work, these 12 measurement errors were excluded from further analysis<sup>6</sup>, leaving four classification errors remaining under the constant speed boundaries.

Figure 3.3 repeats the comparisons from Figure 3.1, only now applied to the actual loop detector data from BHL Station 8. Comparing the two figures, on average the speeds were higher at BHL Station 8, in part because it was towards the upstream end of the NGSIM segment and in part because it comes strictly from the first 15 minute period

---

<sup>5</sup> In general one does not normally know the size of the detection zone without using additional analysis, e.g., Lee and Coifman (2012b). With the BHL data we have the benefit of ground truth length data from NGSIM to eliminate the bias, thereby facilitating direct comparisons between the ground truth and measured lengths for the evaluation, and allowing us to achieve *well tuned detectors* for our analysis. The fact that the detection zone is larger than the physical loops is consistent with the fact that this station also exhibits splashover errors, both factors indicate that the detector sensitivity is set too high.

<sup>6</sup> Both the combined splashover events extending otherwise valid dwell times and the non-vehicle pulses arising from splashover are excluded from the evaluation because they are the result of poorly tuned loop detectors. These errors can be identified using the method in Lee and Coifman (2012a) and the detector station retuned. While we would prefer to work with a well tuned detector station for this evaluation, we only know of this one empirical data set that has both the necessary individual vehicle actuations from the loop detectors during congestion and the concurrent, independently measured ground truth vehicle lengths.

of the NGSIM I-80 dataset, which was the least congested of the three NGSIM time periods at I-80.

Figure 3.4a plots the measured effective vehicle length versus the measured vehicle speed for each of these vehicles, sorted by the true vehicle class as denoted with the given marker symbol. Superimposed on top of this plot are the uncertainty zones from Figure 2.5. Figure 3.4b shows the one misclassification that remains after excluding all of the vehicles that were correctly classified either into a single class or to an uncertainty zone that included the correct class. Table 3.3 quantifies these results. The right-hand side shows the results using CM+ and the conventional constant speed boundaries: only four vehicles are misclassified. For reference, Table 3.4 repeats the evaluation using CM from Equation 2 and the conventional constant speed boundaries. The error rate increases to 5 misclassifications (0.5%, and similar to the corresponding rate in Table 3.2).

The left-hand side of Table 3.3 shows the results from CM+ after accounting for the uncertainty zones. The number of misclassified vehicles when using the uncertainty zones dropped to just one (improved by a factor of 4 over CM+ with the constant speed boundaries). A total of 12 vehicles (1.1%) are assigned to two or more classes in this case.

Table 3.1. Using the synthetic detectors from NGSIM at 1,000 ft, the left-hand side of this table compares the measured length class when including the uncertainty zones against the true length class. The right-hand side of this table repeats a comparison using only the conventional constant speed boundaries between classes.

		using the uncertainty zones							using the conventional constant speed boundaries					
		1	2	3	1,2	2,3	1,2,3	# Errors	Accuracy	1	2	3	# Errors	Accuracy
TRUE	1	5,440	0	0	25	0	1	0	100%	5,463	2	1	3	99.9%
	2	0	63	0	10	6	0	0	100%	0	77	2	2	97.5%
	3	0	1	113	0	10	6	1	99.2%	0	2	128	2	98.5%
	Sum	5,440	64	113	35	16	7	1	total # veh	5,463	81	131	7	total # veh
	Percent	95.9%	1.1%	2.0%	0.6%	0.3%	0.1%	0.02%	5,675	96.3%	1.4%	2.3%	0.1%	5,675

Table 3.2. Repeating the analysis for CM using the synthetic detectors from NGSIM at 1,000 ft, comparing the conventional constant speed boundaries between classes against the true length class.

		using the conventional constant speed boundaries				
		1	2	3	# Errors	Accuracy
TRUE	1	5,440	25	1	26	99.5%
	2	0	76	3	3	96.2%
	3	0	5	125	5	96.2%
Sum		5,440	106	129	34	total # veh
Percent		95.9%	1.9%	2.3%	0.6%	5,675

Table 3.3. Using the real detector data from BHL loop detector Station 8, the left-hand side of this table compares the measured length class when including the uncertainty zones against the true length class. The right-hand side of this table repeats a comparison using only the conventional constant speed boundaries between classes.

		using the uncertainty zones							using the conventional constant speed boundaries					
		1	2	3	1,2	2,3	1,2,3	# Errors	Accuracy	1	2	3	# Errors	Accuracy
TRUE	1	1,021	0	0	6	0	0	0	100%	1,024	3	0	3	99.7%
	2	1	15	0	3	1	0	1	95.0%	0	19	1	1	95.0%
	3	0	0	29	0	2	0	0	100%	0	0	31	0	100%
Sum		1,022	15	29	9	3	0	1	total # veh	1,024	22	32	4	total # veh
Percent		94.8%	1.4%	2.7%	0.8%	0.3%	0.0%	0.09%	1,078	95.0%	2.0%	3.0%	0.4%	1,078

Table 3.4. Repeating the analysis for CM using the real detector data from BHL loop detector Station 8 comparing the conventional constant speed boundaries between classes against the true length class.

		using the conventional constant speed boundaries				
		1	2	3	# Errors	Accuracy
TRUE	1	1,024	3	0	3	99.7%
	2	1	18	1	2	90.0%
	3	0	0	31	0	100%
Sum		1,025	21	32	5	total # veh
Percent		95.1%	1.9%	3.0%	0.5%	1,078

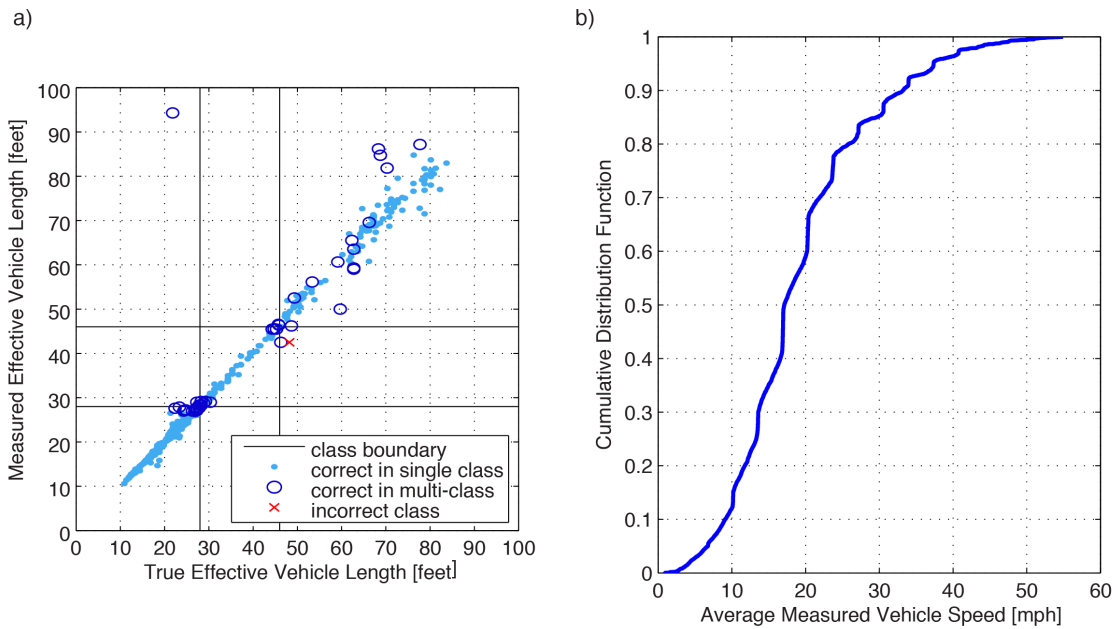


Figure 3.1. (a) Scatter plot comparing the measured length and classification from the synthetic NGSIM detector data versus the true NGSIM length and class at the study location, (b) CDF of average measured speeds for the same vehicles.

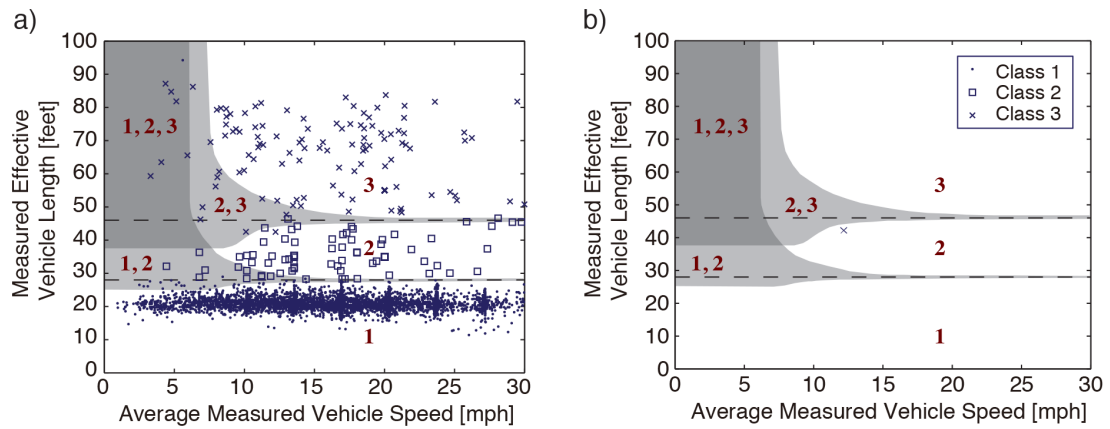


Figure 3.2. (a) Vehicle classification using measured effective vehicle length versus measured speed for all of the NGSIM data at 1,000 ft, (b) repeating part a, but only showing the one misclassification that falls outside of the correct region or uncertainty zones.

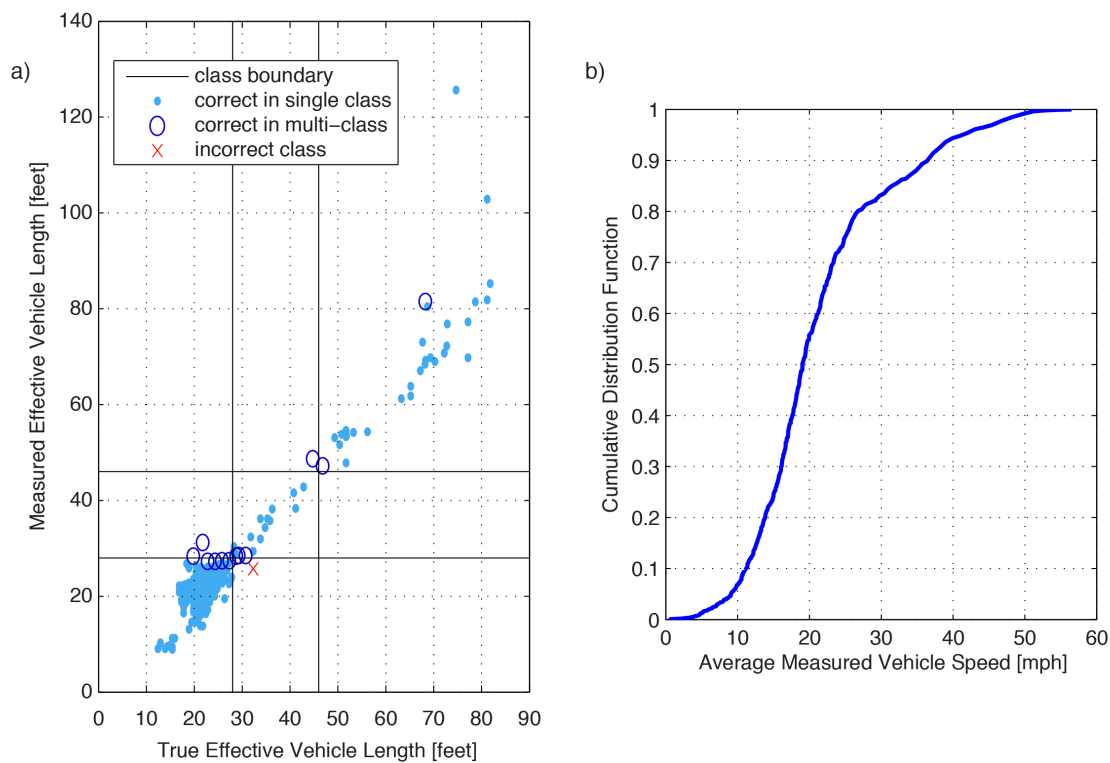


Figure 3.3. (a) Scatter plot comparing the measured length and classification from the real BHL loop detector Station 8 data versus the corresponding true NGSIM length and class, (b) CDF of average measured speeds for the same vehicles.

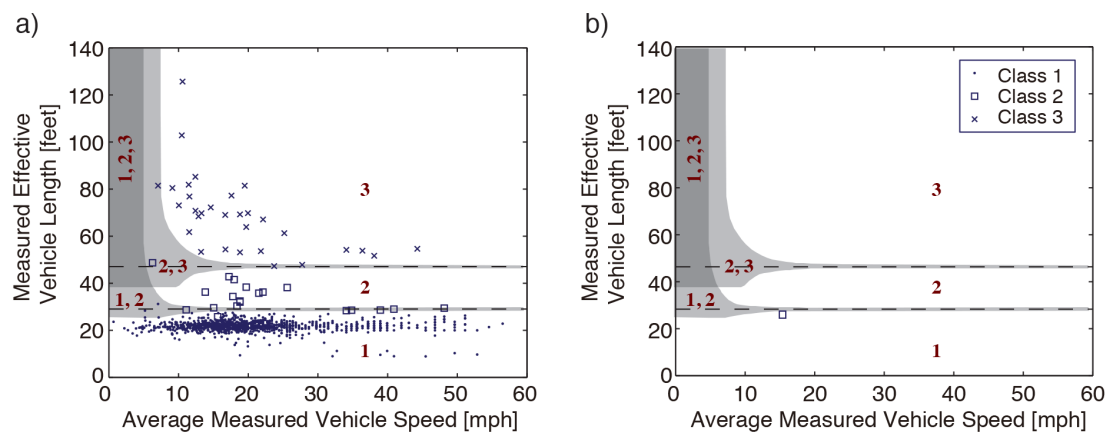


Figure 3.4. (a) Vehicle classification using measured effective vehicle length versus measured speed for all of BHL loop detector Station 8 data, (b) repeating part a, but only showing the one misclassification that falls outside of the correct region or uncertainty zones.

## CHAPTER 4. DISCUSSION AND CONCLUSIONS

Dual loop detectors are among the lowest cost technologies commonly used for collecting vehicle classification data. The conventional approach to classify vehicles at dual loop detectors implicitly assumes that vehicle acceleration is negligible; but unfortunately, at low speeds this assumption is invalid. As a result of this fact, many operating agencies are reluctant to deploy classification stations on roadways where traffic is frequently congested.

This work sought to address the impacts of the unobserved acceleration on the measured length class. After calibration, the approach relies strictly on the measured effective vehicle length and measured speed at a conventional dual loop detector. To this end, the work established the uncertainty regions where the true vehicle class is ambiguous based on what can actually be measured from a dual loop detector. Using the equations of motion this work analytically derived the set of true vehicle lengths, speeds, and accelerations that could give rise to a particular combination of measured speed and measured effective vehicle length from Equations 1 and 3. Of course acceleration cannot be measured from conventional dual loop detectors and this analysis found that there are small uncertainty zones where the measured length class can differ from the true length class, depending on the unobserved acceleration. In other words, a given combination of measured speed and measured effective vehicle length falling in the uncertainty zones could arise from vehicles with different true length classes. In other words, the uncertainty zones capture the impacts of the unmeasured acceleration. Outside of the uncertainty zones, any error in the measured effective vehicle length due to acceleration will not lead to an error in the measured length class. Thus, by mapping these uncertainty zones, most vehicles can be accurately sorted to a single length class, while the few vehicles that fall within the uncertainty zones are assigned to two or more classes. Using empirical data from stop-and-go traffic we found that this new approach assigns over

98% of the vehicles to a single class, and reduces the classification error rate by at least a factor of four relative to the best conventional constant speed boundary method.

Contrary to conventional wisdom we found that the conventional, constant speed boundaries performed surprisingly well down to 15 mph for both of the empirical evaluation datasets. First, recall that we use the best conventional method from Wu and Coifman (in press), CM+ (given by Equation 1). Meanwhile, Wu and Coifman found that the more common CM (given by Equation 2) yielded roughly twice the classification error rate than CM+. Next, as seen in Figure 2.1, almost 60% of the accelerations are within -1 mphps to 1 mphps; thus, the range of accelerations tended to be much closer to zero than was modeled in Figure 2.5. So for vehicles that did not come to a stop over the detectors, the constant speed boundaries were already a pretty good match, as shown in Figure 2.4a with the magnitude of acceleration limited to 1 mphps. Most of the classification errors that did occur using the constant speed boundaries fell within the uncertainty zones predicted by this work, as shown in Tables 1 and 3. As such, the greatest benefits of this work come at the lowest speeds, i.e., below 15 mph. Or alternatively, this work has shown that it is fairly safe to extend conventional length-based dual loop detector vehicle classification down to 15 or 20 mph, provided the detectors are well tuned and one uses CM+ rather than CM (compare Table 3.2 to the right-hand side of Table 3.1).

Comparing the performance from the uncertainty zones for the purely synthetic data derived from the NGSIM dataset against the performance from the real loop detector actuations from BHL Station 8 data we find that the error rate was higher in the real loop detector data even though speeds were also higher. We attribute this outcome to several factors. Both the synthetic data and the real loop detector data exhibited a single misclassification, the smallest non-zero error rate possible. Given the fact that the number of errors has to be an integer, the larger sample size in the synthetic data leads to a smaller error rate for the single error in the dataset. However, the synthetic data precludes the possibility of a detector error while the real data includes detector errors, so the

former should exhibit a slightly lower error rate, which is consistent with our observed error rates.

In practice the biggest problems with length-based vehicle classification often are due to inoperable or malfunctioning detectors rather than the length-based measurement scheme. Which is why it is critically important to make sure the detectors are well tuned. To this end, it is important for an operating agency to follow an established protocol for calibration and to quantify the reliability of the classification system. It is equally important to have an ongoing performance monitoring in real-time to ensure the detectors remain well tuned, e.g., Coifman (1999), Lee and Coifman (2011, 2012a, 2012b). If a detector fails the real-time tests then the corresponding data are of questionable quality and the detector is in need of re-tuning.

The uncertainty zone method presented in this work is meant to extend meaningful length-based vehicle classification to sites that see some congestion. Reviewing the different subplots in Figures 2.2c-d, clearly the stop case and even some of the low speed, non-constant acceleration cases can yield very large errors in the measured effective vehicle lengths. Fortunately, these errors are somewhat rare for several reasons, first, very few vehicles actually pass the dual loop detector at these low speeds, since the lower the speed the lower the flow and the lower the flow the fewer vehicles actually pass a detector. Second, Figure 2.2 shows the errors from the worst case scenario, e.g., the vehicle comes to a stop straddling both loop detectors. If the vehicle stops a few feet further upstream or downstream of this location, straddling just one of the detectors, Wu and Coifman (in press) showed that Equation 1 would yield a much lower effective vehicle length measurement error and this property is the primary reason why CM+ does better than CM. Third, as shown in Figure 2.5, the uncertainty zones only impact measured effective vehicle lengths above 26 ft. There is no uncertainty for any vehicles with a measured effective vehicle length below the zones, no matter how low the measured speed is. As evident in Figures 3.2a and 3.4a, the vast majority of vehicles at these sites are passenger cars, with measured effective vehicle lengths falling below all of the uncertainty zones. Meanwhile, for a measured speed below 8 mph, Figure 2.5 shows

that almost all measured effective vehicle lengths above 26 ft will fall in the uncertainty zones.

The boundaries of the uncertainty zones in Figure 2.5 were derived heuristically in Section 2 for a specific set of length class bins and the given dual loop spacing. The present work seeks to demonstrate just how small the uncertainty zones are. It is left to future work to derive a universal expression to specify the uncertainty zone boundaries for different length bins or dual loop detector spacing. Although we found slightly higher error rates when using the real loop detector data than the purely synthetic data, the difference was very small, i.e., the performance from the NGSIM synthetic transition times was similar to those from the well tuned loop detectors at BHL Station 8. So for some other set of length bins and dual loop spacing, one could simply repeat the analysis of Section 2 and then evaluate the results strictly using the NGSIM data, i.e., repeating Section 3.1. While our work only used the NGSIM I-80 dataset due to the overlap with the BHL, there is a second NGSIM freeway dataset from US-101 that could also be used. In either case, the NGSIM data come from urban freeways with the majority of vehicles being passenger cars. Fortunately, the classification of one vehicle is independent of the classification of another vehicle at a well tuned detector. So if one were interested strictly in the longer vehicles, one could simply discount the class 1 vehicles in Figures 3.2a and 3.4a, and Tables 1 and 3. To increase the proportion of observations arising from long vehicles, the simulated loop detectors could be deployed at multiple locations along one of the NGSIM corridors to generate the synthetic transition data in an effort to sample the limited number of trucks under different acceleration conditions.

## REFERENCES

- Coifman, B. (1999). Using Dual Loop Speed Traps to Identify Detector Errors, *Transportation Research Record 1683*, Transportation Research Board, pp 47-58.
- Coifman, B., Cassidy, M. (2002). Vehicle Reidentification and Travel Time Measurement on Congested Freeways. *Transportation Research- Part A*, 36(10), pp. 899–917.
- Coifman, B., Kim, S. (2009). Speed Estimation and Length Based Vehicle Classification from Freeway Single Loop Detectors. *Transportation Research Part-C*, 17(4), pp 349-364.
- Coifman, B., Lyddy, D., Skabardonis, A. (2000). "The Berkeley Highway Laboratory-Building on the I-880 Field Experiment", *Proc. IEEE ITS Council Annual Meeting*, pp 5-10.
- Davies, P, Salter, D, (1983). "Reliability of Classified Traffic Count Data," *Transportation Research Record 905*, pp 17-27.
- Kim, S., Coifman, B. (2013). "Evaluation of Axle-Based and Length-Based Vehicle Classification Stations," *Transportation Research Record 2339*, pp 1-12.
- Kovvali, V., Alexiadis, V., Zhang, L. (2007). "Video-Based Vehicle Trajectory Data Collection", *Proc. of the 86th Annual TRB Meeting*, TRB.
- Lee, H., Coifman, B. (2011). Identifying and Correcting Pulse-Breakup Errors from Freeway Loop Detectors, *Transportation Research Record 2256*, pp 68-78.
- Lee, H., Coifman, B. (2012a). An Algorithm to Identify Chronic Splashover Errors at Freeway Loop Detectors, *Transportation Research-Part C*. Vol 24, pp 141-156.

- Lee, H., Coifman, B. (2012b). Quantifying Loop Detector Sensitivity and Correcting Detection Problems on Freeways, *ASCE Journal of Transportation Engineering*, Vol. 138, No. 7, pp 871-881.
- Lee, H., Coifman, B., (in press) "Using LIDAR to Validate the Performance of Vehicle Classification Stations," *Journal of Intelligent Transportation Systems*
- Minge, E., Peterson, S., Weinblatt, H., Coifman, B., Hoekman, E., (2012). *Loop- and Length-Based Vehicle Classification, Federal Highway Administration – Pooled Fund Program [TPF-5(192)]*, Final Report, Minnesota Department of Transportation.
- Montanino, M., Punzo, V. (2013). Making NGSIM Data Usable for Studies on Traffic Flow Theory: Multistep Method for Vehicle Trajectory Reconstruction, *Transportation Research Record 2390*, pp 99–111
- Punzo, V., Borzacchiello, M., Ciuffo, B. (2011). On the Assessment of Vehicle Trajectory Data Accuracy and Application to the Next Generation SIMulation (NGSIM) Program Data. *Transportation Research Part C*, Vol. 19, No. 6., pp. 1243-1262.
- Wu L., Coifman, B. (in press). “Vehicle Length Measurement and Classification in Congested Freeway Traffic”, *Transportation Research Record*.